Journal of Industrial and Engineering Chemistry 33 (2016) 162–169

Contents lists available at ScienceDirect

Journal of Industrial and Engineering Chemistry

journal homepage: www.elsevier.com/locate/jiec

Characterization and mechanism analysis of graphite/C-doped TiO_2 composite for enhanced photocatalytic performance

Jialin Jia [a], Dong Li [a], Jiafeng Wan [a,*], Xiujuan Yu [a,b,*]

[a] Department of Environmental Science and Engineering, Heilongjiang University, Xuefu Road 74, Nangang District, Harbin 150080, Heilongjiang Province, PR China

[b] Key Laboratory of Chemical Engineering Process & Technology for High-efficiency Conversion, Harbin, College of Heilongjiang Province, PR China

ARTICLE INFO

Article history:
Received 29 May 2015
Received in revised form 11 August 2015
Accepted 25 September 2015
Available online 9 October 2015

Keywords:
TiO_2
Graphite
C-doping
Photocatalysis
Methyl orange

ABSTRACT

Graphite/C-doped TiO_2 composite was synthesized through a modified sol–gel reaction. DRS results indicated that light absorbance edge of graphite/C-doped TiO_2 was clearly red-shifted to visible light region by doping with C. SPS results displayed that separation efficiency of photoinduced charge carriers of graphite/C-doped TiO_2 were greatly increased by coupling with graphite. Moreover, the photocatalytic performance of composite was evaluated by the degradation of methyl orange (MO). Results showed that graphite/C-doped TiO_2 exhibited higher photocatalytic activity for MO than that of pristine TiO_2 and P25, which was mainly attributed to the high crystallization, large surface hydroxyl groups, intense visible light absorption and effective separation of photoinduced charge carriers.

Introduction

The utilization of solar energy for the stimulation of TiO_2 photocatalyst to degrade pollutants in wastewater has been widely investigated and considered as one of the most promising contamination treatment techniques owing to its characteristic physicochemical properties [1]. Nevertheless, the photocatalytic (PC) activity and practical application of TiO_2 catalyst was restricted because of its intrinsic drawbacks. On the one hand, TiO_2 suffered from the limitation of irradiation wavelengths in the UV region, which only accounts for 4–6% of the solar spectrum [2]. On the other hand, the high recombination rate of photoexcited electrons and holes (e^-/h^+) pairs lowered the quantum efficiency of TiO_2 [3].

Thus, in order to drive effectively the absorption of TiO_2 from the UV light into visible light region and restrain the charge carriers recombination, a great deal of attempts have been done, such as adulteration with nonmetal/metal [4,5], photosensitization with dyes [6], coupling narrow band-gap semiconductor/carbon materials [7–11] and depositing precious metal [12]. In particular, the combination TiO_2 nanomaterials with carbon materials including activated carbon [8], carbon nanotubes [9,12], graphene [10], graphite [11] and carbon doping [5] recently attracted considerable interest and exhibited distinctly potential advantages over other types of modification method, which can be attributed to the following aspects: (a) carbon materials possess metallic conductivity as one of the many possible electronic materials [5,13]; (b) carbon materials hold an intense electron-accepting capacity and can store the photoinduced electrons to prevent the recombination of the photogenerated electron–hole (e^-–h^+) pairs [9,14]; (c) carbon materials presents an intense and wide range of visible light absorption in the range of 400–800 nm, hence aggregating a number of thermal energy which can promote the movement of the photoexcited electrons from the bulk of the TiO_2 into the oxidation reaction sites and further generate a series of active species [15,16]; and (d) C element is always demonstrated transferring into the lattice of TiO_2 through replacing some lattice Ti atoms and forms C–O or C=O bond in the process of carbon doping, which produces a hybrid orbital just below the conduction band of TiO_2 and improves the utilization efficiency of visible light [17,18]. Among these carbon materials, graphite has been attracting considerable attention owing to cheap, available, high temperature resistance, compatibility and the simple and large-scale production relative to other counterparts [11,19]. And the intraplanar π-bands in the graphite consisting of $C2p_z$ orbitals

* Corresponding authors at: Department of Environmental Science and Engineering, Heilongjiang University, Xuefu Road 74, Nangang District, Harbin 150080, Heilongjiang Province, PR China. Tel.: +86 451 86608549; fax: +86 451 86413259.
E-mail addresses: yuxiujuan@hlju.edu.cn, wanjiafeng@hlju.edu.cn (X. Yu).

http://dx.doi.org/10.1016/j.jiec.2015.09.030
1226-086X/

could readily accept electrons [20]. Moreover, graphite would be much more easily to incorporation the C elements into the lattice of TiO_2 than its counterparts such as graphene due to its disordered graphite and impurity carbon.

Under these circumstances, we were combining the efforts of graphite coupling and carbon element doping for the sake of exploit visible light active and efficient TiO_2-based photocatalysts which are easy to manufacture even in industrial quantities. In the present work we showed that a TiO_2-based photocatalyst coupling with graphite and doping with C element could be prepared through a simple modified sol–gel means by the addition of G. Structure, morphology and chemical state of the resulting material were characterized by X-ray diffraction (XRD), scanning electrons microscopy (SEM), transmission electron microscope (TEM) and X-ray photoelectron microscopy (XPS). In addition, the optical property of as-prepared samples was investigated through UV–vis light diffuse reflection spectroscopy (DRS). And the photoinduced charge transfer and separation properties of graphite/C-doped TiO_2 were studied by surface photovoltage spectroscopy (SPS). Moreover, the photocatalytic performance of the as-synthesized graphite/C-doped TiO_2 composite was evaluated by the degradation of MO under Xenon lamp and visible light irradiation. As expected, graphite/C-doped TiO_2 sample exhibited a higher photocatalytic performance than that of pristine TiO_2 and P25 TiO_2. Meanwhile, the photocatalytic performance enhanced mechanism was discussed in detail.

Experimental

Materials

Graphite (G) was purchased from Sinopharm Chemical Reagent Co., Ltd. All the chemicals used in this study were analytical grade and employed without further purification. Deionized (DI) water was used throughout in all our experiments.

Preparation of photocatalysts

Graphite/C-doped TiO_2 composite was prepared through simple one-step sol–gel method as follows. Firstly, 10 mL of tetrabutyl titanate was dissolved into 40 mL of absolute ethanol and stirred for 30 min in a dry atmosphere to get a homogeneous solution, which was denoted as A. And the solution B used as titrant was composed of 10 mL of absolute ethanol and 12 mL of diluted HNO_3 with a volume ratio of 5:1 between deionized water and concentrated nitric acid. Subsequently, solution B was added dropwise into A to obtain solution C under vigorously stirring at room temperature. Afterwards, the desired amount of graphite (0.03 g) was added into the solution C. Next step, the black sol was yielded after continuously vigorous magnetic stirring for 150 min. After the resulting black sol was aged for 24 h and dried at 80 °C in an oven for 48 h, the G/C-doped TiO_2 precursor was generated. Finally, the graphite/C-doped TiO_2 xerogel was grinded in agate mortar into powder and calcinated in a muffle furnace at 350 °C for 2 h with a heating rate of 3 °C/min to obtain nanocrystalline G/C-doped TiO_2. The amount of catalyst produced from above procedure was approximately 9 g. For comparison, the unmodified TiO_2 was also synthesized under the otherwise identical conditions in the absence of graphite.

Characterization of photocatalysts

The resulting materials were characterized by employing various techniques. The crystal structures of the samples were confirmed with the help of X-ray diffraction (XRD-D8 Advance, Bruker) equipped with Cu Kα radiation source (α = 0.15418 nm), at an accelerating voltage of 40 kV, and emission current of 30 mA was employed. The microstructures of the as-prepared G/C-doped TiO_2 composite were recorded by using a field emission scanning electron microscope (FE-SEM, Hitachi S-4800). Transmission electron microscope (TEM) JEOL JEM-2010 at an accelerating voltage of 200 kV was also used to record the electron micrographs of the samples. X-ray photoelectron spectroscopy (XPS) was carried out on a Kratos-AXIS UL TRA DLD with Al Kα X-ray source. All binding energies were calibrated with surface adventitious carbon of 284.6 eV. Ultraviolet-visible diffuse reflectance spectra (DRS) of the samples were conducted with a TU-1901 spectrophotometer, in which $BaSO_4$ was employed as the background ranging from 190 nm to 800 nm. The separation performances of photogenerated charge carriers were tested by a surface photovoltage spectrum (SPS) measurement system with a home-built apparatus equipped with a lock-in amplifier (SR830) synchronized with a light chopper (SR540). The powder sample was sandwiched between two indium tin oxide (ITO) glass electrodes, which were arranged in an atmosphere-controlled container with a quartz window, and a monochromatic light was obtained by passing light from a 500 W xenon lamp (CHF XQ500W, Global xenon lamp power) through a double prism monochromator (SBP300). All of the characterization measurements were performed at room temperature.

Evaluation of photocatalytic performance

To evaluate the photocatalytic performance of various samples, methyl orange (MO) was chosen as model pollutant. The photocatalytic experiments for MO were carried out at room temperature in a 100 mL of home-made cylindrical quartz photoreactor (200 mm × 25 mm, Fig. 1). To measure the photocatalytic activity, for each measurement 50 mg of photocatalysts was taken and dissolved in 30 mL of 10 mg/L MO aqueous solution. A 500 W short arc Xenon lamp equipped with a filter to cut light of wavelengths below 420 nm was used as the visible light source to provide a light intensity of 9.6 Klux, which was placed about 10 cm beside the photoreactor (Fig. 1). Afterwards, the Xenon lamp was turn on for 120 min. Compared to irradiation, the suspension was kept in the dark under magnetic stirring for 120 min to investigate the adsorption behaviors of the photocatalysts. After every

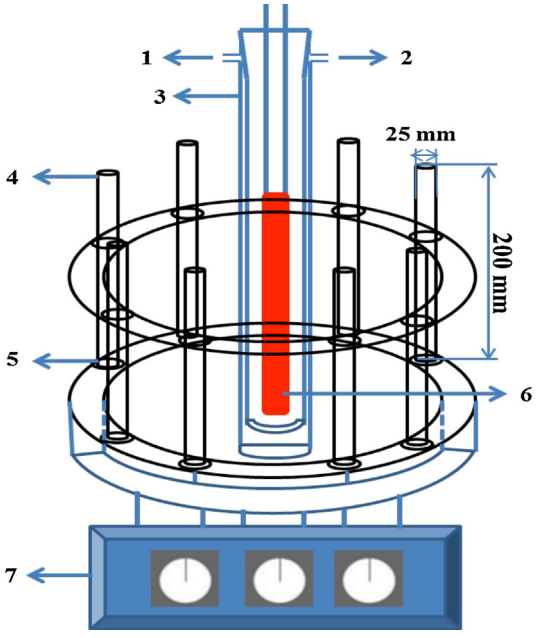

Fig. 1. Schematic diagram of the photoreactor.

120 min photocatalytic reaction, 2 mL of the analytical samples was collected from the suspension, and immediately centrifuging and filtrating to remove the catalyst. Subsequently, the concentration of the collected solutions were measured at λ = 464 nm by using a T6 UV–vis spectrophotometer, from which the photocatalytic degradation rate of MO was calculated. The same experiment was repeated for every sample.

Results and discussion

XRD, SEM and TEM analysis

XRD analysis was carried out to investigate the crystalline phase and structure of the products. Fig. 2 revealed the XRD patterns of as-prepared G, pristine TiO_2 and G/C-doped TiO_2 samples in the region of $2\theta = 10–80^\circ$. Clearly, the characteristic diffraction peaks of the XRD pattern for the G sample at 26.5°, 43.3°, 44.5°, 54.6° and 77.4° were attributed to the (0 0 2), (1 0 0), (1 0 1), (0 0 4) and (1 1 0) planes of G [21], which was in agreement with the 41-1487 standard card from Joint Committee on Powder Diffraction Standards (JCPDS). Notably, pristine TiO_2 and G/C-doped TiO_2 showed formation of anatase (JCPDS file no. 21-1272) phase peaks at $2\theta = 25.3^\circ, 37.8^\circ, 48.1^\circ, 54.5^\circ$, and 62.9° and brookite (JCPDS file no. 29-1360) phase peak at 30.9° with anatase phase in the majority according to their peak intensities. The peak appearing at 26.5° was related to formation of the (0 0 2) plane of G. Meanwhile, the effective grain size of the as-prepared samples was calculated by Debye–Scherrer formula on the anatase (1 0 1) diffraction peaks [22]. The average crystallite sizes of the pristine and G/C-doped TiO_2 samples were found to be 8.8 nm and 9.8 nm, respectively, indicating that introducing with G had an acceleration effect on the growth of crystallite size. Zhu et al. [23] and Dědková et al. [24] also reported that the introduction of graphene and graphite could lead to an increase of TiO_2 nanoparticle size. And the growth phenomenon became increasingly serious as increase of the graphite [24]. Simultaneously, it is worthy of noting that when we used simple modified sol–gel reaction to synthesize G/C-doped TiO_2 composite, it was clear that the crystallization of the G/C-doped TiO_2 composite was better than pristine TiO_2 through comparing the diffraction peak intensity of anatase (1 0 1) plane. The excellent crystallization of the TiO_2 enhanced its photocatalytic activity [25]. Therefore, the G addition for the G/C-doped TiO_2 could affect the crystal properties of the catalysts to a certain extent.

The morphological features of G and G/C-doped TiO_2 composite have been investigated by means of FE-SEM microscopy (see Fig. 3). As shown in Fig. 3a, sample G had irregular morphology of block or flake with smooth surface, which possess block or flake lengths in the range of 1–5μm and wall thickness of 200–500 nm, while the surface of G/C-doped TiO_2 composite exhibited large aggregates of particles made up of much smaller crystallites (Fig. 3b), which were the TiO_2 particles. Magnified image of the dotted line in Fig. 3b was displayed in Fig. 3c. The photographs (Fig. 3c) revealed that TiO_2 consisted of agglomerates of primary particles with average diameter approximately 10 nm. Fig. 4a

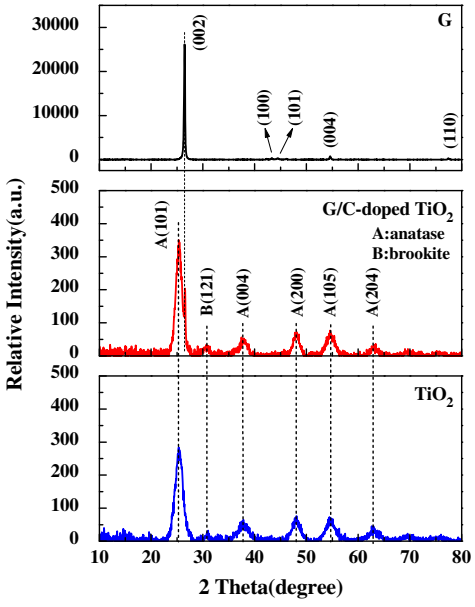

Fig. 2. XRD patterns of TiO_2, G and G/C-doped TiO_2 composite.

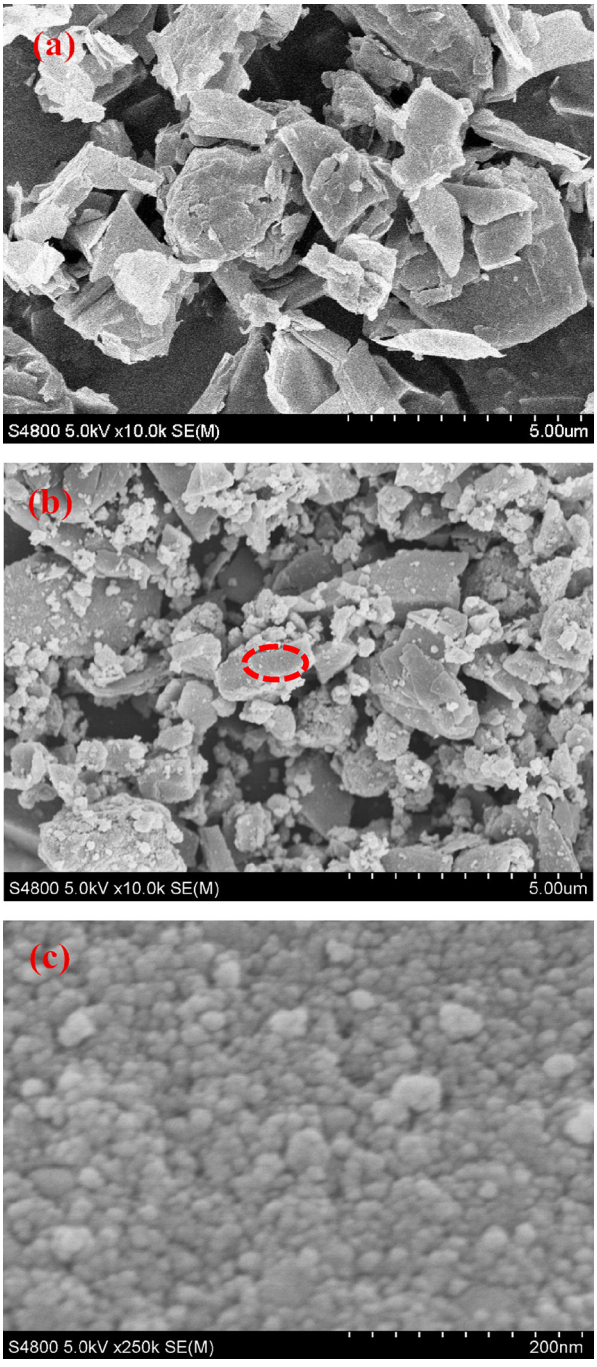

Fig. 3. FE-SEM images of G (a), G/C-doped TiO_2 composite (b, c).

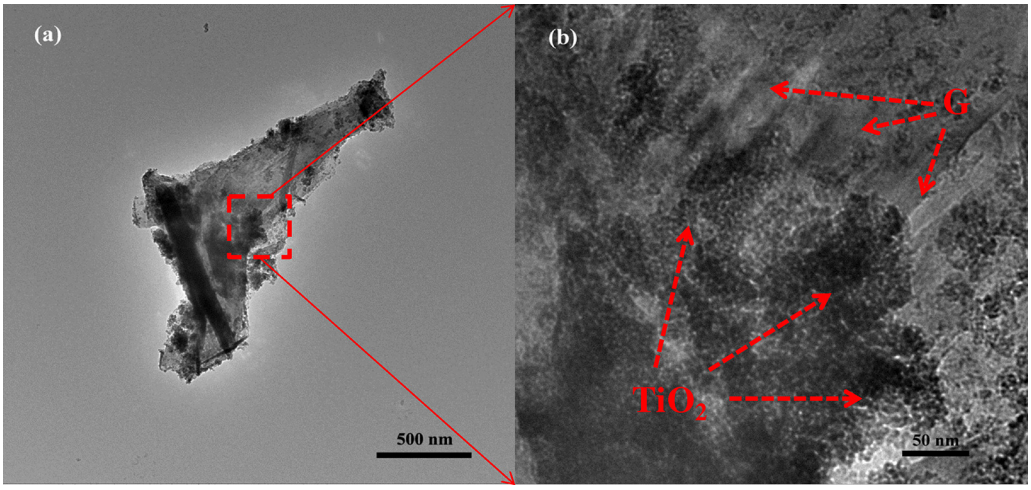

Fig. 4. TEM photographs of G/C-doped TiO_2 composite (a, b).

showed a typical TEM photograph of G/C-doped TiO_2 composite clearly implying many small TiO_2 clusters uniformly deposited on the surface of G with little agglomeration. Fig. 4b presented magnification of approximate area from Fig. 3a outlined in red rectangle, it can be seen that TiO_2 nanoparticles attached onto the surface of G were about 10 nm, which was consistent well with the crystallite size calculated from the XRD characterization and SEM observation.

The XRD, SEM and TEM characterizations indicated that a complete conduction can exist throughout the G/C-doped TiO_2 composite, connecting the TiO_2 nanoparticles to the conducting G. This would allow the irradiated TiO_2 nanoparticles to inject their photoinduced electrons into the G blocks or sheets, reducing the electron–hole recombination thereby improving photocatalytic activity.

XPS analysis

X-ray photoelectron spectroscopy (XPS) with high sensitivity has usually been considered as a powerful and effective technique to investigate the surface composition and chemical states of all kinds of micro/nanomaterials. Fig. 5a exhibited the comparative full-scale XPS survey spectra of the as-prepared undoped TiO_2 and G/C-doped TiO_2 composite. Obviously, both TiO_2 samples contained C, O and Ti elements with sharp binding energies at about 284.6 eV (C1s), 529.6 eV (O1s) and 458.5 eV (Ti2p), respectively. In addition, for pure TiO_2 nanoparticles sample, the atomic composition of C, O and Ti elements was 18.78%, 55.24% and 25.98 at.%, respectively. Nevertheless, the atomic composition of C, O and Ti elements on the surface of G/C-doped TiO_2 composite was 30.14%, 48.55% and 21.32 at.%, respectively, suggesting the markedly increase of C element amount, which was ascribed to the modification of graphite. In order to distinguish the chemical state of C1s in G/C-doped TiO_2 composite, C1s high resolution XPS spectrum was conducted. Noticeable, the C1s binding energy peaks of G/C-doped TiO_2 were broad and asymmetric, demonstrating that there were coexistence of different chemical states of C atoms according to their binding energies ranging from 282 eV to 290 eV as seen from Fig. 5b. After fitting of the curve, six peaks at binding energies of 283.5 eV, 284.1 eV, 284.6 eV, 285.2 eV, 286.1 eV and 288.7 eV were clearly observed, suggesting the existence of six different types of C states. The deconvoluted C1s peak at binding energy of 283.5 eV has already been assigned in the literature to disordered graphite [26]. The two major deconvoluted C1s peaks at 284.1 eV and 284.6 eV were attributed to the presence of sp^2 type C of graphite [26–28], while another major peak at 285.2 eV was assigned to the sp^3 type C graphitic component [26,28], suggesting that graphite was successfully combined together with TiO_2 nanoparticles, which was in accordance with the results of SEM, TEM and XRD results. In addition, the other two C1s peaks appeared at 286.1 eV and 288.7 eV were characteristic of the oxygen bound species C–O and C=O, respectively, demonstrating that C was incorporated into the lattice of TiO_2 by substituting some of the lattice titanium atoms and existed in the form of CO_3^{2-} [17,18], which strongly suggested that the existence of C-doping from the binding energies of the electrons relates to C1s [5,17]. Fig. 5c displayed the high-resolution Ti2p XPS spectrum of the pure TiO_2 and G/C-doped TiO_2 composite. The Ti2p3/2 and Ti2p1/2 core levels of both TiO_2 samples all appeared at about 458.5 eV and 464.3 eV, respectively, indicating that there was no typical suggestion of Ti–C bond formation [29], which were consistent with the C1s XPS analysis. Furthermore, the high resolution XPS spectra of O1s region of pure and G/C-doped TiO_2 were exhibited in Fig. 5d. As seen from this figure, O1s XPS spectra were wide and asymmetric which indicating that there were at least two kinds of chemical states according to the binding energy range from 526 eV to 534 eV, including lattice oxygen and chemiadsorbed oxygen (hydroxyl oxygen) with increasing binding energy [30]. Hence, the O1s XPS spectrum was fitted to two kinds of chemical states and the corresponding XPS data were listed in Table 1. Obviously, the content of hydroxyl oxygen in G/C-doped TiO_2 composite was higher than pure TiO_2, implying that modifying with G made the catalyst possess more surface hydroxyl groups, which favored not only the trapping of electrons to improve the separation efficiency of photogenerated charge carriers but also the forming of surface free radical to enhance the photocatalytic degradation of contaminants [30]. And compared with the O1s binding energies of pure TiO_2, the O1s binding energies for the G/C-doped TiO_2 composite showed an obvious shift toward the higher binding energy, which was also further proved by the fact that the titanium atoms in the lattice of TiO_2 in modified sample may be substituted by carbon atoms, thereby decreasing its probability charge density [17].

Further, the electronic structures of pure and G/C-doped TiO_2 were further investigated by valence band X-ray photoelectron spectroscopy (VBXPS). As seen from Fig. 6, the VB maximum of pure TiO_2 was determined to 2.56 eV by conventional linear extrapolation method, whereas the VB maximum of the G/C-doped

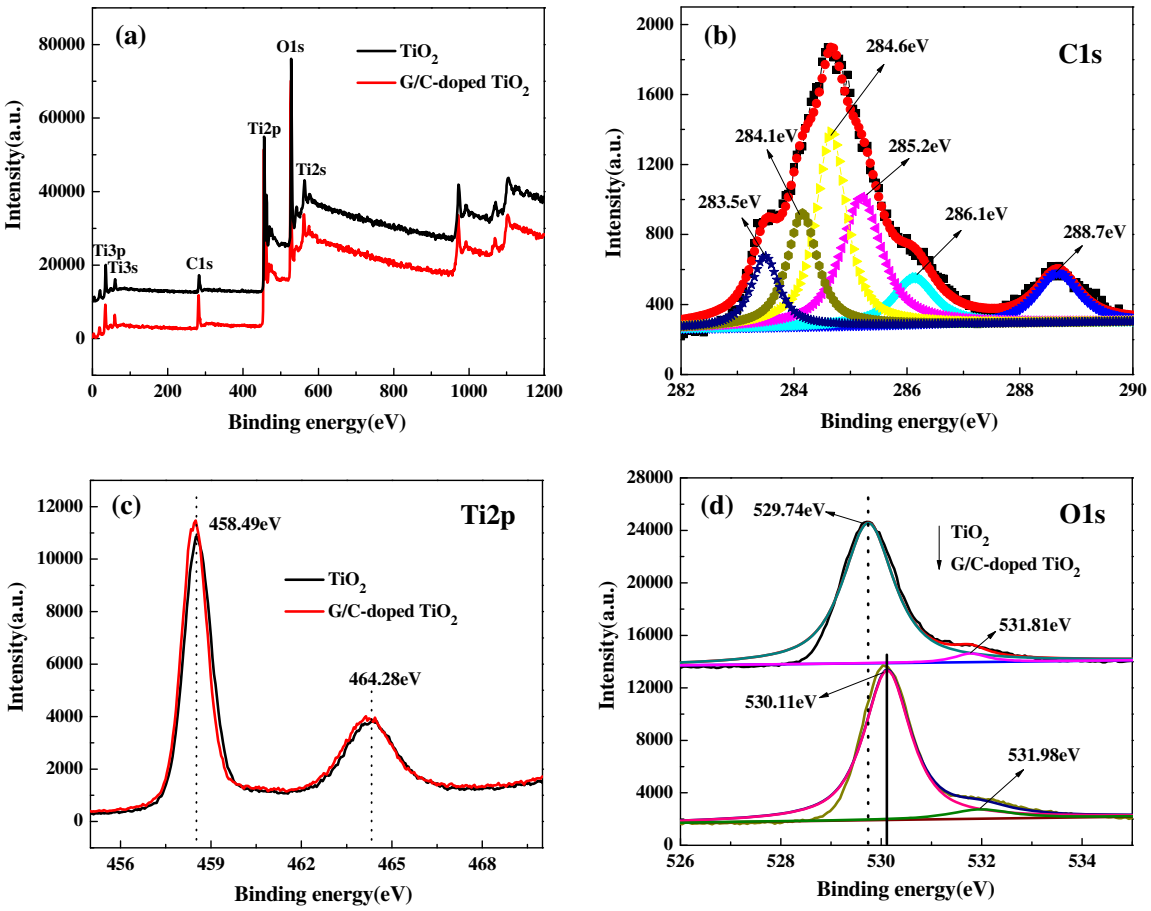

Fig. 5. Survey XPS (a), high-resolution spectra of C1s (b), Ti2p (c) and O1s (d) XPS of the G/C-doped TiO_2 composite.

TiO_2 was noted at 2.17 eV, showing a ~0.39 eV shift to a lower binding energy. This shift of VB was due to the hybridization of 2p orbital of C and 2p orbital of O to form a new valence band in accordance with several other recent reports [31–34]. However, the band gap reduction owing to lowering of CB was reported to be due to formation of the carbonate species, which could induce a new impurity level located the bottom of the conduction band edge [17,35,36]. Therefore, we can conclude that the band gap energy of G/C-doped TiO_2 was smaller. The reduction of the G/C-doped TiO_2 band gap in the present work can therefore be attributed to both the uplift of VB (due to hybridization of C2p and O2p atomic orbits) and lowering of CB (due to carbonate species), suggesting that G/C-doped TiO_2 catalysts should exhibit excellent visible light photocatalytic activity.

DRS and SPS analysis

The UV–vis diffuse reflectance spectra of G, P25, pristine TiO_2, G/C-doped TiO_2 composite samples were recorded and shown in Fig. 7. Noticeably, except G, all the other samples displayed intrinsic absorption spectrum with an intense transition in the UV region of the spectra, corresponding to the electronic transition from O^{2-} anti-bonding orbital to the lowest empty orbital of Ti^{4+}(O2p → Ti3d) [37]. And the G revealed strong photoabsorbance over the entire visible light region. Nevertheless, P25 showed no visible light absorption, while pristine TiO_2 exhibited a little visible light absorption. In comparison with the P25 and pristine TiO_2, the improved absorption in the whole visible light region of the G/C-doped TiO_2 composite can be ascribed to the integration of G. In addition, the absorption edge of G/C-doped TiO_2 composite was slightly shifted to visible light region probably thanks to the formation of C–O or C=O bonds and hybridization of C2p and O2p atomic orbits between the interface of G and TiO_2 [38–40]. The tangent drawn exhibited an absorbance maximum of 397 nm,

Table 1
Curve fitting results of high resolution XPS spectra for the O1s region.

Sample	Lattice oxygen		Hydroxyl oxygen
Pure TiO_2	r (%)	96.2	3.8
	E_b (eV)	529.74	531.81
G/C-doped TiO_2	r (%)	92.4	7.6
	E_b (eV)	530.11	531.98

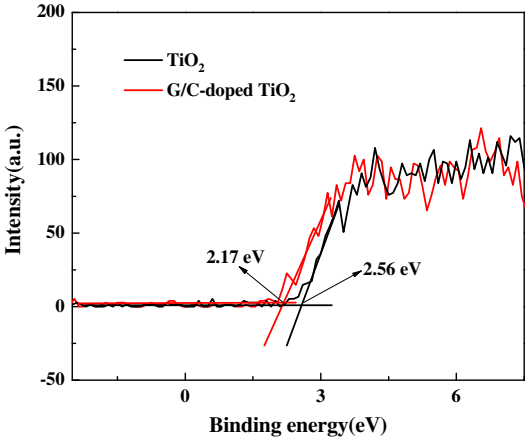

Fig. 6. VBXPS spectra of pure and G/C-doped TiO_2 samples.

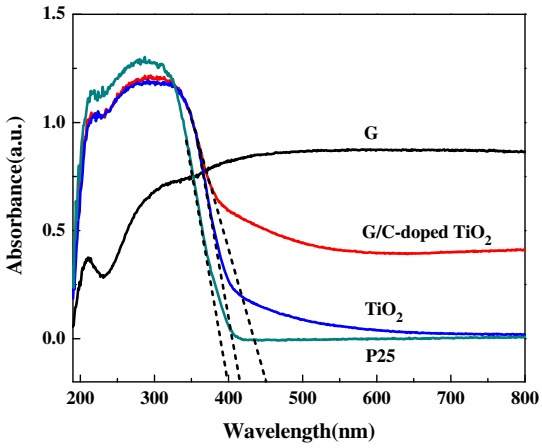

Fig. 7. UV–vis DRS spectra of different TiO_2 samples.

414 nm and 449 nm for the P25, TiO_2 and G/C-doped TiO_2 composite, respectively, which corresponded to a band gap of 3.12 eV, 3.00 eV and 2.76 eV, respectively. This suggested that e^-–h^+ pairs of G/C-doped TiO_2 can be generated, even though the composite was irradiated with long wavelength-visible light. Thus, it can be concluded that modifying with graphite was favorable to induce visible driven photocatalytic reactions.

In order to investigate the effects of surface charge transfer behavior of the pristine TiO_2 and G/C-doped TiO_2 composite, the surface photovoltage spectra (SPS) were measured. Generally speaking, the stronger is the SPS response, the higher is the separation efficiency of photoinduced electron–hole (e^-/h^+) pairs [41,42]. Noticeably, as shown in Fig. 8, both the pristine and G/C-doped TiO_2 samples revealed the obvious SPS signal at about 345 nm, which originated from the electron transition from valence band to conduction band of TiO_2 (band–band transition) [43]. Additionally, a distinct broad SPS signal in the visible-light range of 400–500 nm was observed for G/C-doped TiO_2 composite, which corresponded to the sub-band-gap transition caused by existence of new energy level [44]. In comparison with pristine TiO_2, the G/C-doped TiO_2 composite displayed stronger SPS response at the wavelength of 300–500 nm, indicating that G/C-doped TiO_2 possessed the higher separation rate of photogenerated charge carriers than that of TiO_2, which can be attributed mainly by the following three reasons: (a) the increase of crystallinity gave rise to the reduction of crystal defects of structure so that enhance the built-in electric field strength, meanwhile resulting in the decrease in the recombination chance of photoinduced electrons and holes pairs, therefore facilitating the charge separation and migration [43,45]; (b) the addition of graphite as suitable electronic conductors could accept the photoinduced electrons from TiO_2 to facilitate charge collection and charge transport [39,46]; (c) the incorporation of graphite could generate new energy level by carbon doping and hybridization of C2p and O2p atomic orbits (O2p–C2p). As a result, the photogenerated electrons could easily transfer from the valence band and O2p–C2p energy level to the localized C1s states of TiO_2, which can enhance the separation efficiency of photogenerated charge carriers. Therefore, it can be deduced that G/C-doped TiO_2 composite should possess higher visible light photocatalytic activity than that of pure TiO_2.

Photocatalytic performance

Photocatalytic performances of the as-prepared TiO_2 and G/C-doped TiO_2 samples were investigated by photocatalytic degradation of methyl orange (MO) under Xenon lamp irradiation. The adsorption of MO in dark and the photocatalysis of MO over the P25 were measured as control, and the reduction of MO through directing photolysis was so low (<2%) that it can be neglected. As shown in Fig. 9, it is clear to observe that the photocatalytic degradation efficiency could be greatly improved by coupling with graphite and doping with carbon, which was consistent with the results mentioned above. And the photocatalytic degradation rate of all the TiO_2 samples can be ranged in the following order: G/C-doped TiO_2 > pristine TiO_2 > P25. That is, G/C-doped TiO_2 composite presented the highest photocatalytic performance, for which 77.5% of MO can be decomposed after 120 min of Xenon lamp irradiation. And the photocatalytic efficiencies of home-made TiO_2 and P25 were 45.4%, and 39.1%, respectively. The improvement of photocatalytic activity can be explained by the fact that modification with graphite could promote the transfer and separation of photogenerated charge carriers, enlarge visible light absorption and increase anatase crystallinity, as well as improve content of surface hydroxyl groups. The photocatalytic performance of the pristine TiO_2 and G/C-doped TiO_2 samples under visible light were also investigated by comparing the photocatalytic degradation of MO upon visible light ($\lambda > 420$ nm). It could be seen from Fig. 9 that the G/C-doped TiO_2 composite displayed a little higher photocatalytic activity (35.8%) in contrast to pristine TiO_2 (21.3%) and P25 (21.9%) under visible light irradiation, which primarily based on the visible light excited separation of electrons and holes thanks to the decrease of band gap. In addition, the removal efficiency of MO over the P25, TiO_2 and G/C-doped TiO_2 resulted from adsorption in dark within 120 min were 11.5%, 8.2% and 8.5%, respectively.

Based on the above analysis, the enhanced visible light photocatalytic mechanisms were proposed and illustrated in

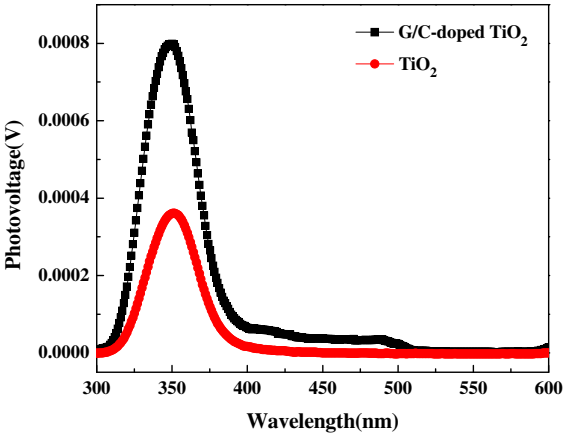

Fig. 8. SPS spectra of TiO_2 and G/C-doped TiO_2 samples.

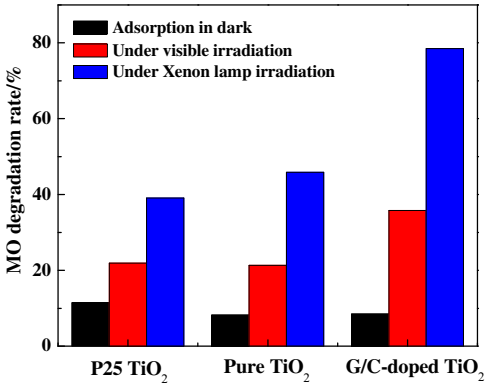

Fig. 9. Photocatalytic degradation rate of MO on different TiO_2 samples.

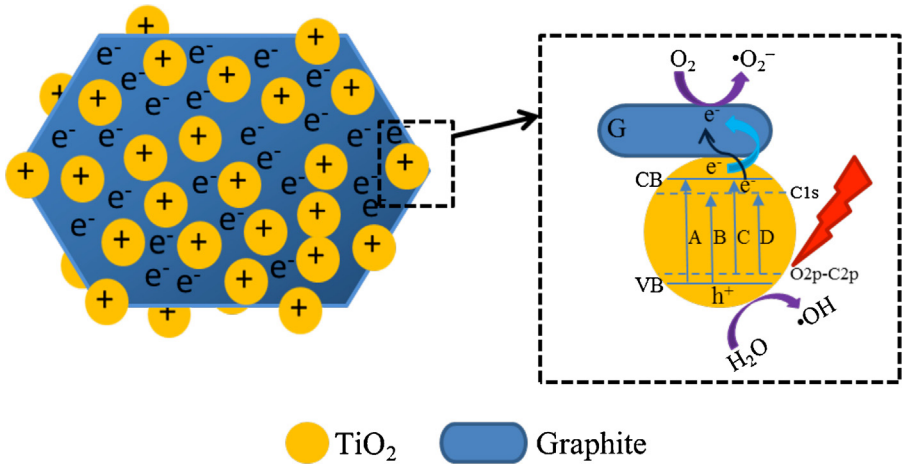

Fig. 10. Scheme of photocatalytic mechanism of G/C-doped TiO_2 composite.

Fig. 10. As shown in Fig. 10, with the substitution for Ti atoms by C in the lattice of TiO_2 and the hybridization of C2p and O2p atomic orbits, new impurity levels (C1s and O2p–C2p) were introduced between the valence band and conduction band of TiO_2. Pure TiO_2 exhibited low photocatalytic activity for the degradation of pollutants due to its wide band gap (3.00 eV process A). As for the modified composite, electrons can be excited from valence band to the C1s doping energy level (process B). The electrons can also be promoted from the hybridization of C2p and O2p atomic orbits energy level to the conduction band (process C). Besides these, the more photogenerated electrons can also be promoted from the localized O2p–C2p energy level to the C1s energy level (process D). In addition, it is possible that the generated electrons could migrate from conduction band and C1s impurity level of TiO_2 to the graphite, resulting in a high separation efficiency of photoinduced charge carriers. As a result, more photogenerated electrons and holes could effectively participate in the photocatalytic reactions, therefore resulting in a higher photocatalytic performance than that of pristine TiO_2 and P25 samples.

Conclusions

In summary, an efficient photocatalyst graphite/C-doped TiO_2 was successfully prepared through a simple sol–gel method, which displayed a higher photocatalytic activity than that of pristine TiO_2 and P25 under Xenon lamp and visible light irradiation. XPS analysis indicated that a small amount of C atoms were incorporated into the lattice of TiO_2 by cationic substitution type C doping and graphite was mainly the presence of sp^2 and sp^3 type C graphitic component. The incorporation of graphite with TiO_2 nanocrystalline enhanced the anatase crystallization and visible photons absorption and reduced the recombination rate of photogenerated electron–hole pairs. The G/C-doped TiO_2 composite showed a marked enhanced photocatalytic performance for degradation of MO, which was mainly attributed to the well anatase crystallinity, intense light absorption in visible region, narrow band gap and more content of surface hydroxyl groups, as well as the better charge separation and collection efficiency. This work may provide a new way to large-scale synthesize TiO_2-based photocatalyst effectively working for wastewater remediation applications.

Acknowledgments

This work was supported by National Natural Science Foundation of China for Youth (21106035) and Youth Scholar Backbone Supporting Plan Project for General Colleges and Universities of Heilongjiang province (1151G034), and Key Laboratory of Chemical Engineering Process & Technology for High-efficiency Conversion.

References

[1] M.Y. Wang, J. Ioccozia, L. Sun, C.J. Lin, Z.Q. Lin, Energy Environ. Sci. 7 (2014) 2182.
[2] S.A. Ansari, M.M. Khan, M.O. Ansari, M.H. Cho, Sol. Energy Mater. Sol. Cells 141 (2015) 162.
[3] J. Di, S. Li, Z. Zhao, Y. Huang, Y. Jia, H. Zheng, Chem. Eng. J. 281 (2015) 60.
[4] K. Pathakoti, S. Morrow, C. Han, M. Pelaez, X. He, D.D. Dionysiou, H.M. Hwang, Environ. Sci. Technol. 47 (2013) 9988.
[5] Y. Zhang, Z. Zhao, J. Chen, L. Cheng, J. Chang, W. Sheng, C. Hu, S. Cao, Appl. Catal. B: Environ. 165 (2015) 715.
[6] M. Liang, J. Chen, Chem. Soc. Rev. 42 (2013) 3453.
[7] T. Ghosh, K.Y. Cho, K. Ullah, V. Nikam, C.Y. Park, Z.D. Meng, W.C. Oh, J. Ind. Eng. Chem. 19 (2013) 797–805.
[8] M.H. Baek, W.C. Jung, J.W. Yoon, J.S. Hong, Y.S. Lee, J.K. Suh, J. Ind. Eng. Chem. 19 (2013) 469.
[9] A. Kongkanand, P.V. Kamat, ACS Nano 1 (2007) 13.
[10] K. Ullah, Z.D. Meng, S. Ye, L. Zhu, W.C. Oh, J. Ind. Eng. Chem. 20 (2014) 1035.
[11] G. Palmisano, V. Loddo, H.H. El Nazer, S. Yurdakal, V. Augugliaro, R. Ciriminna, M. Pagliaro, Chem. Eng. J. 155 (2009) 339.
[12] R.M. Mohamed, I.A. Mkhalid, J. Ind. Eng. Chem. 22 (2015) 390.
[13] K. Woan, G. Pyrgiotakis, W. Sigmund, Adv. Mater. 21 (2009) 2233.
[14] G. Zhang, F. Teng, Y. Wang, P. Zhang, C. Gong, L. Chen, C. Zhao, E. Xie, RSC Adv. 3 (2013) 24644.
[15] Z. He, W. Que, Y. He, RSC Adv. 4 (2014) 3332.
[16] S. Lee, Y. Lee, D.H. Kim, J. Moon, ACS Appl. Mater. Interf. 5 (2013) 12526.
[17] D. Li, Z. Xing, X. Yu, X. Cheng, Electrochim. Acta 170 (2015) 182.
[18] I.A. Appavoo, J. Hu, Y. Huang, S.F.Y. Li, S.L. Ong, Water Res. 57 (2014) 270.
[19] J.H. Li, L.L. Feng, Z.X. Jia, Mater. Lett. 60 (2006) 746.
[20] Z.H. Wang, S.M. Selbach, T. Grande, RSC Adv. 4 (2014) 4069.
[21] H. Panjiar, R.P. Gakkhar, B.S.S. Daniel, Powder Technol. 275 (2015) 25.
[22] Q. Chen, H. Liu, Y. Xin, X. Cheng, Electrochim. Acta 111 (2013) 284.
[23] L. Zhu, S.B. Jo, S. Ye, K. Ullah, Z.D. Meng, W.C. Oh, J. Ind. Eng. Chem. 22 (2015) 264.
[24] K. Dědková, J. Lang, K. Matějová, P. Peikertová, J. Holešinský, V. Vodárek, J. Kukutschová, J. Photochem. Photobiol. B 149 (2015) 265.
[25] S.T. Nishanthia, S. Iyyapushpama, B. Sundarakannana, E. Subramanianb, D. Pathinettam Padiyan, Appl. Surf. Sci. 313 (2014) 449.
[26] T. Paulmier, J.M. Bell, P.M. Fredericks, Thin Solid Films 515 (2007) 2926.
[27] O. Akhavan, M. Abdolahad, A. Esfandiar, M. Mohatashamifar, J. Phys. Chem. C 114 (2010) 12955.
[28] X.C. LeQuan, W.P. Kang, J.L. Davidson, B.K. Choi, Y.M. Wong, R. Barbosa, W. Lu, Diamond Relat. Mater. 18 (2009) 200.
[29] E.M. Neville, M.J. Mattle, D. Loughrey, B. Rajesh, M. Rahman, J.M. Don MacElroy, J.A. Sullivan, K.R. Thampi, J. Phys. Chem. C 116 (2012) 16511.
[30] X. Cheng, H. Liu, Q. Chen, J. Li, P. Wang, Electrochim. Acta 103 (2013) 134.
[31] K.X. Li, J.J. Xiong, T. Chen, L.S. Yan, Y.H. Dai, D.Y. Song, J. Hazard. Mater. 250–251 (2013) 19.
[32] M.Q. Yang, N. Zhang, Y.J. Xu, ACS Appl. Mater. Int. 5 (3) (2013) 1156.
[33] D. Maruthamani, D. Divakar, M. Kumaravel, J. Ind. Eng. Chem. (2015), http://dx.doi.org/10.1016/j.jiec.2015.04.026.
[34] Y. Lin, C. Weng, F. Chen, Chem. Eng. J. 248 (2014) 175.
[35] H. Kamisaka, T. Adachi, K. Yamashita, J. Chem. Phys. 123 (2005) 084704.
[36] X. Cheng, X. Yu, Z. Xing, J. Phys. Chem. Solids 74 (2013) 684.
[37] D. Li, X. Cheng, X. Yu, Z. Xing, Chem. Eng. J. 279 (2015) 994.

[38] Y.H. Zhang, Z.R. Tang, X.Z. Fu, Y.J. Xu, ACS Nano 4 (2010) 7303.
[39] X. Yu, Y. Zhang, X. Cheng, Electrochim. Acta 137 (2014) 668.
[40] Y. Zhang, Z. Zhou, T. Chen, H. Wang, W. Lu, J. Environ. Sci. 26 (2014) 2114.
[41] M. Humayun, A. Zada, Z. Li, M. Xie, X. Zhang, Y. Qu, F. Raziq, L. Jing, Appl. Catal. B: Environ. 180 (2016) 219.
[42] P. Luan, M. Xie, X. Fu, Y. Qu, X. Sun, L. Jing, Phys. Chem. Chem. Phys. 17 (2015) 5043.
[43] L. Jing, W. Zhou, G. Tian, H. Fu, Chem. Soc. Rev. 42 (2013) 9509.
[44] H. Li, D. Wang, H. Fan, P. Wang, T. Jiang, T. Xie, J. Colloid Interf. Sci. 354 (2011) 175.
[45] X. Cheng, X. Yu, Z. Xing, Appl. Surf. Sci. 258 (2012) 3244.
[46] X. Yu, X. Han, Z. Zhao, J. Zhang, W. Guo, C. Pan, A. Li, H. Liu, Z.L. Wang, Nano Energy 11 (2015) 19.